

Nanoparticles actively fragment armored droplets

François Sicard^{1,*}, Jhoan Toro-Mendoza², and Alberto Striolo³

¹ *Department of Chemistry, King's College London, SE1 1DB London, United Kingdom*

² *Instituto Venezolano de Investigaciones Científicas,*

Centro de Estudios Interdisciplinarios de la Física, Caracas, Venezuela and

³ *Department of Chemical Engineering, University College London, WC1E 7JE London, United Kingdom*

Understanding the complexity of fragmentation processes is essential for regulating intercellular communication in mechanistic biology and developing novel bottom-up approaches in a large range of multiphase flow processes. In this context, self-fragmentation proceeds without any external mechanical energy input allowing one to create efficiently micro- and nanodroplets. Here we examine self-fragmentation in emulsion nanodroplets stabilized by solid particles with different surface features. Mesoscopic modelling and accelerated dynamics simulations allow us to overcome the limitations of atomistic simulations and offer detailed insight into the interplay between the evolution of the droplet shape and the particle finite-sized effects at the interface. We show that finite-sized nanoparticles play an *active* role in the necking breakup, behaving like nano-scale razors, and affect strongly the thermodynamic properties of the system. The role played by the particles during self-fragmentation might be of relevance to multifunctional biomaterial design and tuning of signaling pathways in mechanistic biology.

Emulsion droplets are metastable dispersions comprised of two immiscible fluids such as water and oil [1, 2]. The associated surface tension forces them into a spherical shape to minimize the free-energy. To decrease the latter and stabilize the emulsion droplets a surface-active agent can be added [3, 4]. Pickering emulsions are stabilized by the incorporation of particles [3, 5]. For instance, emulsion droplets can serve as ideal compartments for reactions catalysed by nanoparticles (NPs) attached at the oil-water interfaces [6], can be used as drug-delivery vehicles [7], sensors [8] and templates for the fabrication of advanced functional materials [9]. The characteristics of Pickering emulsions pose a number of intriguing fundamental physical questions including a thorough understanding of the perennial lack of detail about how particles arrange at the liquid/liquid interface. Other not completely answered questions include particle effects on interfacial tension [10], layering [11], buckling [12] and droplet bridging [13]. Interestingly, emulsion droplets show some relevant characteristics and qualities of living systems that could make them proxies for artificial life. They provide an experimental framework for synthetic biology that is different from other protocell model systems such as vesicles offering distinct advantages [14–16]. For instance, the apparent similarity in surface properties between inorganic NPs and globular proteins [17] and the fluid dynamical properties of droplets could be combined with different chemistries to target applications and exploration of biological scenarios not easily achievable with other supramolecular platforms [18], including the mechanical biology of enveloped viruses such as the rapidly spreading Zika virus [19–21].

In the presence of colloidal particles, the stability of emulsions against fragmentation under ultrasonication [22–24] or shear stress [25, 26] has been a subject of strong interest either at the molecular or mesoscopic

level. However, despite the vast interest in particle-laden interfaces, less is known about the self-fragmentation mechanism, *i.e.* fragmentation without any external mechanical energy input. Tcholakova *et al.* [27] studied self-emulsification process via cooling-heating cycles causing repeating breakup of droplets to higher-energy states. However, this approach relies on small changes in temperature affecting the spontaneous curvature due to surfactant thermally-activated modification. We are here interested in self-fragmentation at constant temperature, as it is observed in the proliferation of living cells [14–16, 18].

Due to their inherent limited resolution, direct access to local observables, such as the particles' three-phase contact angle distribution, the measure of decrease in interfacial tension with the decrease in droplet size, as characterized by the Tolman length [28], or the presence of particles remain out of reach. These pieces of information can be accessed by numerical simulations. All-atom molecular dynamics (MD) simulations have become a widely employed computational technique. However, all-atom MD simulations are computationally expensive. Moreover, most phenomena of interest can take place on time scales that are orders of magnitude longer than those accessible via all-atom MD. Mesoscopic simulations, in which the structural unit is a coarse-grained representation of a large number of molecules, and enhanced sampling techniques allow us to overcome these limitations. Coarse-grained approaches offer the possibility of answering fundamental questions responsible for the collective behaviour of particles anchored at an interface [29].

We employ here Dissipative Particle Dynamics (DPD) as a mesoscopic simulation method [31] along with accelerated dynamics simulations [32] to study

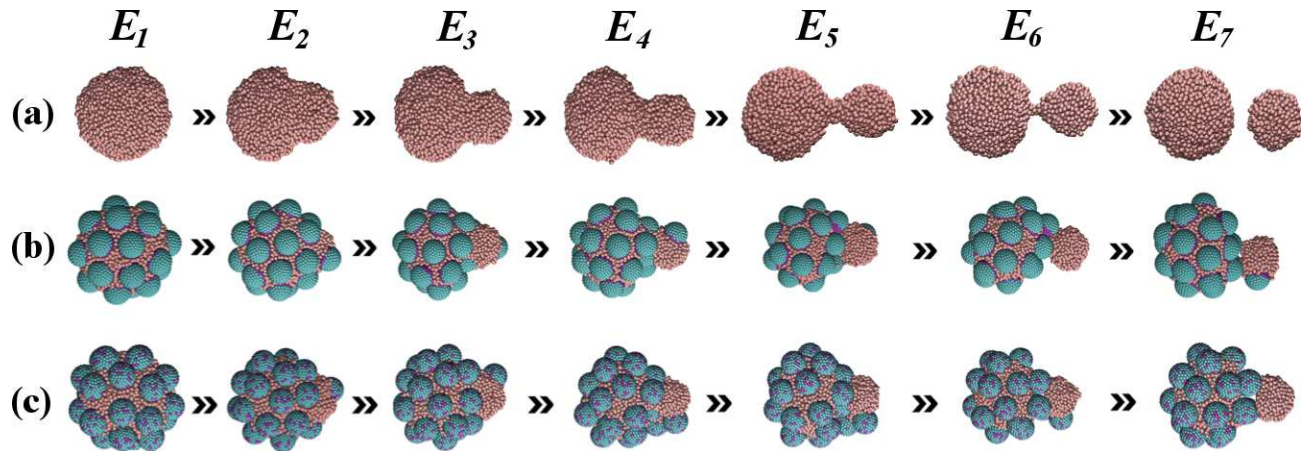


FIG. 1. Sequence of simulation snapshots representing the *thermally-assisted* self-fragmentation processes of water in oil nanodroplets in the bare configuration (a) or armored with 24 spherical Janus (b) and homogeneous (c) NPs. The bare and armored nanodroplets are constituted of the same number of water beads, $N_W \approx 3500$. The same NP surface coverage $\phi \approx 0.9$, as defined in Ref. [30], is considered on the armored nanodroplets. The NPs simulated have the same volume, $4/3\pi a_0^3$, where $a_0 \approx 1.5$ nm. This yields the radius of gyration, $R_{GYR} = (3.764 \pm 0.004)$ nm, and $R_{GYR} = (3.953 \pm 0.008)$ nm for bare and armored nanodroplets, respectively. Cyan and purple spheres represent polar and apolar beads. Pink spheres represent water beads. The oil beads surrounding the droplets are not shown for clarity. The number of contacts, N_C (see Methods), decreases from left to right, with E_1 corresponding to the *original* configuration and E_7 to the final configuration obtained within the accelerated dynamics framework.

accurately the free-energy landscapes and the necking breakup mechanisms associated with *thermally-assisted* self-fragmentation of model water nanodroplets coated with spherical NPs and immersed in an organic solvent. The scale temperature in the DPD framework is equivalent to 298.73 K. The procedure and parametrisation details are described in the Supplementary Information (SI). The particles are of two types: Janus (particles whose surface shows two distinct wetting properties) and homogeneous (particles with one surface characteristic). They are chosen so that the initial three-phase contact angles ($\approx 90^\circ$) result in maximum adsorption energy [33]. To study the thermodynamic properties of the self-fragmentation mechanism and the role played by the finite-sized particles, we combined several enhanced sampling frameworks, metadynamics (metaD) [34], umbrella sampling (US) [35], and adiabatic biased molecular dynamics (ABMD) [36, 37]. To take into account the inherent fluid nature of the system, we designed a *dynamic* collective variable (CV) allowing to bias unequivocally the dynamics of the system based on dynamical labelling of the fluid molecules composing the emulsion droplet as well as the *mother* and the *daughter* emulsion droplets resulting from self-fragmentation (see Methods). We consider throughout this study the same number of fluid molecules constituting the bare or armored emulsion nanodroplets, and the same NP density on the armored nanodroplets.

In Fig. 1 we show representative snapshots obtained in the accelerated dynamics simulations for the bare emul-

sion nanodroplet (panel a) and a system stabilized with either Janus (panel b) or homogenous (panel c) NPs. Starting with the spherical bare droplet (configuration E_1 in Fig. 1a), the system fragments with the formation of a liquid bridge whose shape approximately describes an evolving parabola (E_2 to E_6). The curvature of the liquid bridge increases continuously along the fragmentation process until *mother* and *daughter* nanodroplets separate, resulting in two distinct emulsion nanodroplets with radius of gyration $R_{GYR}^{(m)} = (3.521 \pm 0.004)$ nm and $R_{GYR}^{(d)} = (2.188 \pm 0.007)$ nm, respectively (E_7).

The fragmentation process is fundamentally different when the emulsion droplet is stabilized with either Janus

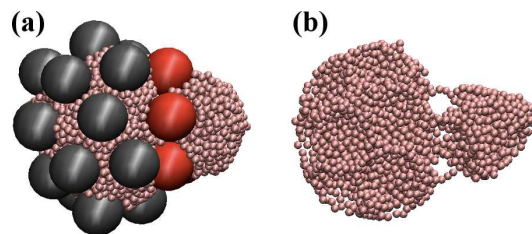


FIG. 2. Simulation snapshot obtained during the *thermally-assisted* self-fragmentation process of the emulsion droplet armored with Janus NPs. (a) The edging NPs separating *mother* and *daughter* droplets are coloured in red. The particles which are not involved in the fragmentation process are coloured in grey. (b) Illustration of the filament bridge formed in the necking breakup mechanism when the particles in panel (a) are not shown. Pink spheres represent water beads. The oil beads are not shown for clarity.

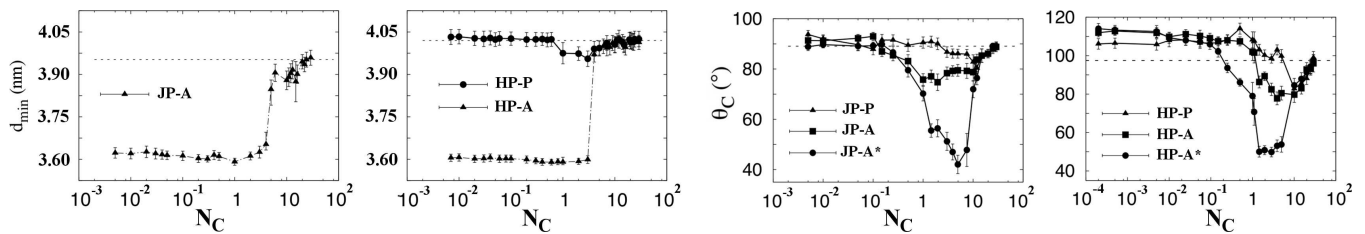


FIG. 3. Evolution of the representative minimal distances d_{min} (left panels) measured between the edging NPs and the representative three-phase contact angles θ_C (right panels) of Janus (JP) and homogeneous (HP) edging NPs as a function of the number of contacts N_C between *mother* and *daughter* droplets (see Methods). The letters *P* and *A* are used to differentiate the NPs which play a *passive* and an *active* role in the breakup mechanism, respectively. The statistical errors are estimated as one standard deviation from the average as obtained for equilibrated trajectories. The values d_{min} and θ_C of a representative NP far from the fragmentation area are plotted in dashed line for reference.

or homogeneous NPs (cf. Figs. 1b and 1c). As the particles remain strongly adsorbed at the interface during fragmentation, forming a close-packed monolayer, the emulsion nanodroplet fragments forming first a liquid bridge similar to the one observed in the bare droplet (configuration E_2 in Fig. 1). Progressively, the particles located at the fragmentation edge *actively* control the process. They decrease the number of contacts between *mother* and *daughter* droplets. As shown in Fig. 2, these edging NPs control the shape of the bridge between the 2 droplets, behaving like nano-scale razors, and transform the liquid bridge in bridging filaments. Finally, the bridging filaments vanish and *mother* and *daughter* emulsion droplets separate.

When the armored nanodroplet is coated with Janus NPs (panel b), their hydrophobic regions interact with the *daughter* droplet, pushing it further away from the *mother* droplet. The final configuration is fundamentally different when the water nanodroplet is stabilized with homogeneous NPs (panel c). Their specific feature allows the edging NPs to adsorb both at the *mother* and *daughter* droplet interfaces once they are separated, resulting in bridging [37]. Remarkably, as the distance between *mother* and *daughter* droplets is not sufficiently large, the fragmented emulsion droplets can coalesce.

The breakup mechanism just discussed is quantitatively investigated in Fig. 3 (left panels), where we show the evolution of a representative set of minimal distances, d_{min} , measured between the edging NPs separating *mother* and *daughter* nanodroplets as a function of the number of contacts, N_C , between the water molecules in each droplets. The initial distributions of the minimal distances can be described with Gaussian distributions for both Janus (J) and homogeneous (H) NPs. The values of the respective means, μ^J and μ^H , and standard deviations, σ^J and σ^H , differ due to the NP features. We obtain $\mu^J = 3.96$ nm and $\mu^H = 4.02$ nm, and $\sigma^J = 0.03$ nm and $\sigma^H = 0.02$ nm. As the number of contacts N_C between *mother* and *daughter* droplets coated with Janus NPs decreases, the minimal

distances between the edging NPs show two distinct regimes separated with a transition at $N_C^* \approx 5$. When $N_C > N_C^*$, d_{min} decreases slowly as the liquid bridge forms, similar to the one observed in the bare droplet. When $N_C \approx N_C^*$, d_{min} shows a significant jump which is characteristic of the transition from the liquid bridge to the bridging filaments shown in Fig. 2. When $N_C < N_C^*$, d_{min} decreases continuously until the bridging filaments vanish at $N_C^\dagger \approx 1$ and *mother* and *daughter* droplets separate. For $N_C < N_C^\dagger$, d_{min} increases slightly until a plateau is reached, which is characteristic of the local rearrangement of the edging NPs near the fragmentation area. The evolution of the system is qualitatively similar when homogeneous NPs are present, albeit some subtle differences are present due to the NP features. As shown in Fig. 3, two distinct behaviours are observed. Unlike Janus edging NPs, certain homogeneous NPs do not present a distance d_{min} showing a significant jump when $N_C = N_C^*$ but follow a relatively small and continuous decrease for $N_C > N_C^\dagger$. The rest of the evolution is similar to the one observed for Janus NPs, with the continuous increase of d_{min} to the plateau characteristic of the local equilibrium rearrangement of the edging NPs.

This analysis can be completed by quantifying the evolution of the three-phase contact angles, θ_C , of the edging NPs, as shown in Fig. 3 (right panels). The initial distribution can be described with Gaussian distributions for both Janus (J) and homogeneous (H) NPs, with respective means and standard deviations $\mu^J = 89.1^\circ$ and $\mu^H = 97.5^\circ$, and $\sigma^J = 1.6^\circ$ and $\sigma^H = 3.5^\circ$. As the number of contacts N_C between *mother* and *daughter* droplets coated either with Janus or homogeneous NPs decreases, two distinct behaviours emerged, which could discriminate the *active* or *passive* role played by the edging NPs in the self-fragmentation process. When $N_C > N_C^*$, the three-phase contact angle decreases slowly as the liquid bridge forms. When $N_C^\dagger < N_C < N_C^*$, we observe two different evolutions of the contact angle. Some NPs show a continuous and

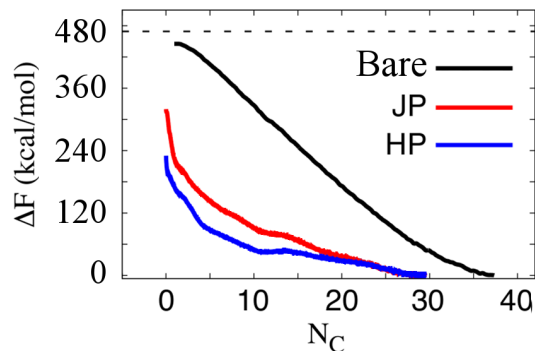


FIG. 4. Free-energy profiles associated with *thermally-assisted* self-fragmentation of the bare and armored droplets as a function of the number of contacts N_C between *mother* and *daughter* droplets (see Methods). The Gibbs free-energy calculated without the Tolman correction is shown as a dashed horizontal line. The positions of the global minima of the bare and armored droplets along N_C differ due to the presence of the particles.

significant decrease of θ_C , with a decrease of $\approx 20\%$ (index A in Fig. 3) and $\approx 50\%$ (index A^* in Fig. 3). This behaviour is representative of the *active* role played by some edging NPs which behave like nano-scale razors. Eventually, the bridging filaments vanish when $N_C = N_C^\dagger$ and *mother* and *daughter* droplets separate for $N_C > N_C^\dagger$. This step is characterized by a significant increase of the contact angle until it reaches a plateau associated with the local rearrangement of the edging NPs resulting in higher value of the contact angles near the fragmentation area. In contrast, some edging NPs show an increase of their contact angle when $N_C < N_C^*$, until it reaches the plateau, characteristic of their *passive* role during the breakup mechanism (index P in Fig. 3).

Finally, building on accelerated dynamics frameworks [32], we assessed the free-energy of self-fragmentation for bare and armored nanodroplets. Considering first the bare droplet, we obtained $\Delta F_B = (445 \pm 3)$ kcal/mol. This value can be compared with the expression of the Gibbs free-energy [38], $\Delta F = \gamma \Delta A$, with γ and ΔA the liquid-liquid interfacial tension and the change in interfacial area, respectively. Taking into account the effect of the curvature of the emulsion nanodroplet [28, 39], one must consider $\gamma = \gamma_0 / (1 + 2\delta/R_S)$ with γ_0 , R_S , and δ denoting the planar interfacial tension, the radius of the surface under tension, and the Tolman length, respectively. Given the interfacial tension for a planar decane/water interface [40], $\gamma_0 = 51.7 \text{ mN.m}^{-1}$, we obtained $\Delta F_0 = (467 \pm 5)$ kcal/mol, which yields the value of the Tolman length $\delta \approx 10^{-8}$ cm, in agreement with the original paper of Tolman [28]. Noticeably, this latter result was directly obtained from our simulations and not as a condition imposed where a definition of surface density profiles are needed in atomistic descriptions.

In Fig. 4, we compared this result with the free-energy of self-fragmentation for the armored nanodroplets, ΔF_J and ΔF_H , respectively, also obtained within the accelerated dynamics framework. As we could expect from the quantitative analysis above, which highlighted the active role played by the finite-sized NPs in the breakup mechanism, we measured $\Delta F_J = (316 \pm 7)$ kcal/mol and $\Delta F_H = (227 \pm 3)$ kcal/mol, significantly lower than the free-energy of self-fragmentation measured for the bare nanodroplet. Furthermore, particle adsorption at the two interfaces when homogeneous NPs are present must be taken into account to estimate the fragmentation free-energy. To do so, we measured the three-phase contact angle of the edging NPs and defined the final fragmentation stage as the one where the edging NPs remain adsorbed at a single interface. In Fig. 5, we show the evolution of the representative three-phase contact angles of the edging NPs with respect to the *daughter* droplet as the fragmentation process progresses from stage E_4 to E_7 , as shown in Fig. 1. As the edging particles HP_1 and HP_2 are fully desorbed when the number of contacts $N_C \approx 10^{-2}$, with a three-phase contact angle $\theta_C = 180^\circ$, two particles, HP_3 and HP_4 , have a contact angle $\theta_C < 180^\circ$ characteristic of particles partially adsorbed at the *daughter* interface. In the Pieranski-Binks approach [33, 41], the change in energy accompanying the desorption of a spherical particle from the interface to either bulk phase can be approximated by $\Delta E = \pi r^2 \gamma_0 (1 \pm \cos \theta)^2$, in which r is the particle radius and the plus (minus) sign refers to desorption into oil (water). Even if this expression assumes that the oil-water interface remains planar, it yields a rough approximation of the energy at play. Considering the contact angles given in Fig. 5, we obtain a correction factor $\Delta \Delta F_H \approx 5$ kcal/mol.

Interestingly, the difference in chemistry of the spherical NPs had some important impact in the reduction of

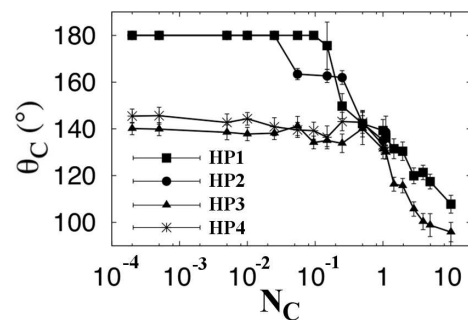


FIG. 5. Representative three-phase contact angles θ_C of the homogeneous (HP) edging NPs with respect to the *daughter* droplet as the fragmentation process progresses from stage E_4 to E_7 as a function of the continuous number of contacts N_C between *mother* and *daughter* droplets (see Methods). The statistical errors are estimated as one standard deviation from the average obtained for equilibrated trajectories.

the free-energy barrier. Unlike Janus NPs, which present a preferred orientation at the liquid-liquid interface resulting in restricted rotational mobility, homogeneous NPs are characterized by larger rotational freedom. This provides the homogeneous NPs with the capability to share easily the interfacial area delimiting *mother* and *daughter* nanodroplets during the fragmentation process. In contrast, when Janus NPs are present, the main energy consumption comes from the *daughter* droplet trying to maintain the orientation of the edging NPs, thus increasing the free-energy of self-fragmentation.

The physical insights discussed in this letter provide a deeper understanding of the organisation of finite-sized NPs at fluid interfaces, and allow us to decipher the *active* or *passive* role played by the particles in the self-fragmentation process. This information could be useful for a variety of applications including multifunctional biomaterial design and tuning of signaling pathways in mechanistic biology, including membrane-bound and membrane-less organelles undergoing apoptosis [42–44]. Apoptosis is a form of programmed cell death that is a highly regulated and controlled biological process [45], which can alter organelle structure and function [42]. Its original role is to kill infected, abnormal, or otherwise undesired cells. There is a long list of diseases associated with altered cell survival. Increased apoptosis is characteristic of AIDS, and neurodegenerative diseases such as Alzheimer’s and Parkinson’s diseases. Decreased or inhibited apoptosis, on the other hand, is a feature of many malignancies, autoimmune disorders, and some viral infections [46]. For instance, increasing evidence suggests that cell-derived extracellular vesicles (EV) produced during apoptosis have important immune regulatory roles relevant across different disease settings [47]. The formation of EVs during apoptosis could be a key mechanism of immune modulation. With most cancer treatments focusing on inducing apoptosis in tumor cells [48], it becomes important to understand selective ways to influence cell differentiation and death. Nanoscale chemistry and topography could act synergistically for better understanding of hidden mechanisms of nanomaterial-induced cell behaviors. From this perspective, emulsion droplets can promote more open thinking about how non-living matter might self-organize into evolving matter that adapts over time to a changing environment.

The extensive simulations discussed above allowed us to decipher *thermally-assisted* self-fragmentation of armored nanodroplet along with the mechanisms at play in the necking breakup process. We showed that finite-sized NPs can play an *active* role, behaving like nano-scale razors, during the evolution of the droplet shape and affect strongly the stability of the system, resulting in significant reduction of the fragmentation free-energy ranging between 150 – 250 kcal/mol, which is equivalent to the

energy released by 20 – 30 ATP molecules [49]. The DPD framework considered in this work would allow extending these results to a range of bio-inspired liquid-liquid systems where the adsorption of the particles does not lead to a significant deformation of the interface. This is a valid approximation for particles ranging from nanometer to micrometer size [29]. These properties might be of relevance for the control and/or tuning of the fragmentation of cell-derived extracellular vesicles, which have important immune regulatory roles [44], and bacterial membrane vesicles that affect diverse biological processes, including virulence, phage infection, and cell-to-cell communication [50]. They might also pave the way for new types of nanoscale platforms in synthetic biology to modify the molecular workings of enveloped viruses such as the rapidly spreading Zika virus whose recent outbreak has been linked to microcephaly and Guillain-Barré syndrome [19–21].

ACKNOWLEDGEMENTS

The authors acknowledge V. Garbin, and L. Botto for useful discussions. F.S. thanks M. Salvalaglio for fruitful discussion concerning the accelerated dynamics frameworks and P. Rousseau, A. Lesne, and M. Barbi for stimulating discussions regarding the biological implications of our findings. Via our membership of the UKs HEC Materials Chemistry Consortium, which is funded by EPSRC (EP/L000202), this work used the ARCHER UK National Supercomputing Service (<http://www.archer.ac.uk>). F.S. acknowledges the support of the UK Engineering and Physical Sciences Research Council (EPSRC), under grant number 527889.

METHODS

Dynamical coordination number. To take into account the inherent fluid nature of the system, *i.e.* the absence of covalent interactions between the molecules of the fluids, we designed a *dynamic* collective variable (CV) which allowed us to bias unequivocally the dynamics of the system based on dynamical labelling of the fluid molecules composing *mother* and *daughter* droplets resulting from the self-fragmentation process. In this optic, we considered the MULTICOLVAR module of the plugin for free-energy calculation, PLUMED, version 2.3 [51].

- We first arbitrarily aligned the principal axis of deformation of the system with the *Z*-Cartesian axis of the the DPD simulation box.
- We settled the *fragmentation center* as our reference position in the Cartesian space using a virtual atom in a fixed position with the `FIXEDATOM` function available in PLUMED [51].

- We used the function ZDISTANCES to calculate the Z-components of the vectors connecting the fluid molecules constituting the droplet and the *fragmentation center*.
- We filtered the distribution of distances obtained with the ZDISTANCES function to *dynamically* discriminate the molecules located on the right (left) side of the *fragmentation center*. To do so, we used the function MFILTER_MORE (MFILTER_LESS) implemented in PLUMED [51] to create these two dynamic groups.
- Thereafter, we fixed the number of molecules constituting *mother* and *daughter* droplets. To do so, we used the RESTRAINT function implemented in PLUMED [51] which can add harmonic and/or linear restraints on specific CVs. We applied the RESTRAINT function on two dynamic groups defined with the options LESS_THAN and MORE_THAN implemented in the ZDISTANCES function.
- We computed the number of contacts, N_C , between the two dynamic groups previously defined with MFILTER_MORE and MFILTER_LESS using the function COORDINATIONNUMBER implemented in PLUMED [51]. This variable counts the number of contacts between two groups of atoms and is defined as $N_C = \sum_i \sum_j s_{ij}$ with $s_{ij} = 1$ if the contact between atoms i and j is formed and $s_{ij} = 0$ otherwise. To make N_C differentiable s_{ij} is replaced with a switching function. We considered the RATIONAL switching function $s(r) = \frac{1 - (\frac{r - D_0}{R_0})^n}{1 - (\frac{r - D_0}{R_0})^m}$, with $n = 6$ and $m = 12$. We choose $D_0 = 0.6375$ nm, as obtained from the position of the first peak of the radial distribution function calculated from the distances between the fluid molecules, which correspond to the first coordination shell of the system [51]. We then tuned the value of the parameter $R_0 = 0.8625$ nm to allow the *daughter* droplet to separate completely from the *mother* droplet during fragmentation.
- Finally, we defined the continuous number of contacts as the mean value of the COORDINATIONNUMBER discussed above. To do so, we used the MEAN option implemented in the MULTICOLVAR module available in PLUMED [51].

* Corresponding author: francois.sicard@free.fr.

[1] F. Leal-Calderon and P. Poulin, Curr. Opin. Colloid. Interface Sci. **4**, 223 (1999).
 [2] L. Shu, J. Eijkel, and A. van den Berg, Adv. Colloid Interface Sci. **133**, 35 (2007).

[3] B. Binks, Curr. Opin. Colloid Interface Sci. **7**, 21 (2002).
 [4] B. Binks and A. Desforges, Langmuir **23**, 1098 (2007).
 [5] S. Pickering, J. Chem. Soc., Trans. **91**, 2001 (1907).
 [6] Y. Qu, R. Huang, W. Q. Qu, R. Su, and Z. He, Part. Part. Syst. Charact. **34**, 1700117 (2017).
 [7] J. Frelichowska, M.-A. Bolzinger, J.-P. Valour, H. Mouaziz, J. Pelletier, and Y. Chevalier, Int. J. Pharm. **23**, 7 (2009).
 [8] M. Pan, M. Kim, L. Blauch, and S. Tang, RSC Adv. **6**, 39926 (2016).
 [9] M. Agrawal, S. Gupta, and M. Stamm, J. Mater. Chem. **21**, 615 (2011).
 [10] R. Miller, V. Fainerman, V. Kovalchuk, D. Grigoriev, M. Leser, and M. Michel, Adv. Colloid Interface Sci. **128-130**, 17 (2006).
 [11] S. Razavi, K. Cao, B. Lin, K. Lee, and R. Tu, Langmuir **31**, 7764 (2015).
 [12] F. Sicard and A. Striolo, Nanoscale **9**, 8567 (2017).
 [13] N. Bizmark and M. Ioannidis, Soft Matter **14**, 6404 (2018).
 [14] T. Ichii, H. Suzuki, and T. Yomo, EPL **96**, 48006 (2011).
 [15] F. Caschera, S. Rasmussen, and M. Hanczyc, Chem. Plus Chem. **78**, 52 (2013).
 [16] D. Zwicker, R. Seyboldt, C. Weber, A. Hyman, and F. Julicher, Nature Physics **13**, 408 (2017).
 [17] N. Kotov, Science **330**, 188 (2010).
 [18] M. Hanczyc, Life **4**, 1038 (2014).
 [19] V. Sikka, V. K. Chattu, R. Popli, S. Galwankar, D. Kelkar, S. Sawicki, S. Stawicki, and T. Papadimos, J. Glob. Infect. Dis. **8**, 3 (2016).
 [20] M. Sevvana, F. Long, A. Miller, T. Klose, G. Buda, L. Sun, R. Kuhn, and M. Rossmann, Structure **26**, 1169 (2018).
 [21] T. H. Saey, ScienceNews **194**, 15 (2018).
 [22] K. Ramisetty and R. Shyamsunder, Int. J. Drug Delivery **3**, 133 (2011).
 [23] V. Lad and Z. Murthy, Ind. Eng. Chem. Res. **51**, 4222 (2012).
 [24] A. Huerre, M. Corato, and V. Garbin, Nature Communication **9**, 3620 (2018).
 [25] C. Mabile, F. Leal-Calderon, J. Bibette, and V. Schmitt, urophys. Lett. **61**, 708 (2003).
 [26] M. Mulligan and J. Rothstein, Langmuir **27**, 9760 (2011).
 [27] S.Tcholakova, Z. Valkova, D. Cholakova, Z. Vinarov, I. Lesov, N. Denkov, and S. Smoukov, Nature Communications **8**, 15012 (2017).
 [28] R. Tolman, J. Chem. Phys. **17**, 333 (1949).
 [29] N. Wu, D. Lee, and A. Striolo, Anisotropic Particle Assemblies: Synthesis, Assembly, Modeling, and (Elsevier, Amsterdam, 2018).
 [30] X.-C. Luu, J. Yu, and A. Striolo, Langmuir **29**, 7221 (2013).
 [31] R. Groot and P. Warren, J. Chem. Phys. **107**, 4423 (1997).
 [32] D. Hamelberg, J. Mongan, and J. McCammon, J. Chem. Phys. **120**, 11919 (2004).
 [33] B. Binks and S. Lumsdon, Langmuir **16**, 8622 (2000).
 [34] A. Laio and M. Parrinello, Proc. Nat. Acad. Soc. U.S.A. **99**, 1256212566 (2002).
 [35] J. Kastner, Wiley Interdiscip. Rev.: Comput. Mol. Sci. **1**, 932 (2011).
 [36] M. Marchi and P. Ballone, J. Chem. Phys. **110**, 3697 (1999).
 [37] F. Sicard and A. Striolo, Faraday Discuss. **191**, 287

- (2016).
- [38] P.-G. de Gennes, F. Brochard-Wyart, and D. Quere, *Capillarity and Wetting Phenomena: Drops, Bubbles, Pearls* (Springer-Verlag, New York, USA, 2004).
- [39] Y. Lei, T. Bykov, S. Yoo, and X. Zeng, *J. Am. Chem. Soc.* **127**, 15346 (2005).
- [40] H. Fan and A. Striolo, *Phys. Rev. E* **86**, 051610 (2012).
- [41] H. Wi, S. Cingarapu, K. Klabunde, and B. Law, *Langmuir* **27**, 9979 (2011).
- [42] M. G. Bottone, G. Santin, F. Aredia, G. Bernocchi, C. Pellicciari, and A. Scovassi, *Cells* **2**, 294 (2013).
- [43] A. Aguilera-Gomez and C. Rabouille, *Developmental Biology* **428**, 310 (2017).
- [44] J. Chen and L. Stark, *Cells* **7**, 157 (2018).
- [45] S. Elmore, *Toxicologic Pathology* **35**, 495 (2007).
- [46] A. Renehan, C. Booth, and C. Potten, *BMJ* **322**, 1536 (2001).
- [47] S. Caruso and K. Poon, *Front. Immunol.* **9**, 1486 (2018).
- [48] R. Wong, *J Exp Clin Cancer Res.* **30**, 87 (2011).
- [49] E. Gajewski, D. Steckler, and R. Goldberg, *J. Biol. Chem.* **261**, 1273312737 (1986).
- [50] M. Toyofuku, N. Nomura, and L. Eberl, *Nature Reviews Microbiology* **17**, 13 (2019).
- [51] G. Tribello, M. Bonomi, D. Branduardi, C. Camilloni, and G. Bussi, *Comput. Phys. Commun.* **185**, 604613 (2014).